Nano Energy 123 (2024) 109357

Contents lists available at ScienceDirect

Nano Energy

journal homepage: www.elsevier.com/locate/nanoen

Bionic octopus-like flexible three-dimensional force sensor for meticulous handwriting recognition in human-computer interactions

Diqing Ruan [a], Guanzheng Chen [a], Xuanzi Luo [a], Lin Cheng [a,*], Huaping Wu [b,*], Aiping Liu [a,*]

[a] Key Laboratory of Optical Field Manipulation of Zhejiang Province, College of science, Zhejiang Sci-Tech University, Hangzhou 310018, China
[b] Key Laboratory of Special Purpose Equipment and Advanced Processing Technology, Ministry of Education and Zhejiang Province, College of Mechanical Engineering, Zhejiang University of Technology, Hangzhou 310023, China

ARTICLE INFO

Keywords:
Flexible sensor
Three-dimensional force
Bionic octopus-structure
Handwriting recognition
Neural network

ABSTRACT

With the advantages of high flexibility, multifunctional integration, and wearing comfort, flexible tactile sensors hold great potential for application in the field of intelligent sensing system and human-computer interaction. However, the high sensitivity acquisition and the issue of decoupling of complex tactile signals, and improving compatibility of flexible tactile sensors in human-computer interfaces are still serious challenges in current research. In this study, drawing inspiration from the body structure of an octopus, we developed a flexible three-dimensional (3D) force sensor in which a CNT/Ecoflex conductive elastomer as the body of the bionic octopus-like sensor could capture the normal component of 3D spatial force, meanwhile a laser-induced graphene sensing film transferred to Ecoflex (LIG/Ecoflex) as the tactile wrists of the bionic octopus sensor could discern the magnitude and direction of the tangential component of the 3D spatial force. The bionic sensor offered excellent sensing and wearable characteristics, including fast and efficient response, cyclic stability, and flexible skin-fit performance. The unique structural design of the sensor enabled spatial force sensing capability and precise decoupling and output of 3D forces through the use of a multilayer perceptron (MLP) for mapping and calibration. The octopus-inspired flexible 3D force sensors were further attached to the fingertips of human fingers for successful extraction of handwriting minutia of wearer, showcasing their promising potential in areas such as smart wearables, handwriting recognition, and interactive human-computer interfaces.

1. Introduction

Human-computer interaction (HCI) technology is rapidly advancing in today scientific, technological, and engineering landscapes. Its core aim is to enable more natural, efficient, and accurate interactions between humans and digital systems, enhancing work efficiency, improving quality of life, and pushing forward the boundaries of science and technology [1–5]. This requires advanced sensor preparation and manufacturing technology. Flexible tactile sensors, with their high adaptability, multi-functional integration, lightweight nature, and comfort in wearables, hold immense potential in the field of smart wearable devices and their associated human-computer interactions [6–10]. For instance, Xu et al. demonstrated an ultrathin flexible tactile sensor based on a few-layer graphene film, and developed a flexible smart panel to successfully reproduce a two-dimensional touch path [11]. Choi et al. demonstrated a smart glove by integrating fiber-based tactile sensors [12], which could distinguish the strain, pressure, and bending of fingers by monitoring the single and mutual resistance of twisted fibers as a control interface for virtual shooting games.

In order to improve the sensitivity and authenticity of the flexible tactile sensors in the process of recognizing and sensing human behavior, significant progress has been made in the design of sensor composition, structure and function [13–16]. Especially, biological lives with micro-nano structure in nature always have ultrasensitive senses due to the efficiently evolved structures and organizations [17–19]. Thus, natural world provides us an effective model for the developing of high-performed tactile sensors [20,21]. For instance, Pang et al. demonstrated a high-sensitive strain sensors based on interlocked nanofiber arrays, by mimicking the wing-to-body locking microstructures in beetles [22]. Kang et al. developed a highly functional sensor based on nanoscale crack junctions, inspired by the crack-like slit organs in spiders [23]. Utilizing the structure-activity relationship of helix and radial difference microstructures in spider webs as inspiration, Liu et al. designed and printed graphene porous and dense stacked

* Corresponding authors.
E-mail addresses: chenglin@zstu.edu.cn (L. Cheng), wuhuaping@gmail.com (H. Wu), liuaiping1979@gmail.com (A. Liu).

https://doi.org/10.1016/j.nanoen.2024.109357
Received 12 December 2023; Received in revised form 20 January 2024; Accepted 2 February 2024
Available online 8 February 2024

microstructures to integrate multi-resolution graphene tactile sensors [24]. However, the aforementioned tactile sensors only enhance sensitivity of external stimulus in one-dimensional (1D) force direction, which may not suffice for practical complicated applications. For instance, in the real writing process, the style and strength of writing has individual differences [25,26]. Thus, the development of flexible tactile sensors capable of three-dimensional (3D) force sensing for the precise and accurate identification is a pressing necessity. Chen et al. reported on a flexible 3D force sensor mimicking the interlocking structure of human skin [27]. The sensor's shear direction was achieved via an in-plane triaxial structural arrangement, with a shear angle resolution of less than 30° and a normal force sensitivity of 6.33 kPa^{-1}. The study by Zhou et al. succeeded in decomposing the 3D force onto the bottom pressure-sensitive element, which could be equivalent to the 3D force [28]. However, the design required a flat test surface, limiting its application scope significantly. Zhao et al. designed a flexible two-parameter pressure-strain sensor inspired by spider webs, capable of simultaneously monitoring the magnitude and direction of the applied force [29]. However, this work did not perform complete force decoupling.

To satisfy the need of flexible tactile sensor' s for high sensitivity acquisition of complex tactile signals, accurate decoupling, and superior compatibility in human-computer interfaces, we develop a flexible 3D force sensor with bionic octopus-structure. As the octopus is a representative of a highly evolved mollusk, it possesses a highly developed and centralized nervous system, primarily composed of cerebral nerves in the body and a secondary nervous system in tactile wrists. The ingenious body structure and neuron distribution empower the octopus to sensitively perceive and promptly respond to external stimuli, thereby allowing it to adapt effectively to the complex and dynamic marine environment [30–34]. Drawing inspiration from the octopus, we design a CNT/Ecoflex conductive elastomer as the body of the bionic octopus-like sensor, which can collect the normal component of the 3D spatial force, meanwhile a laser-induced graphene sensing film transferred to Ecoflex (LIG/Ecoflex) as the tactile wrists of the bionic octopus-like sensor, which can discern the magnitude and direction of the tangential component of the 3D spatial force (Fig. 1a). Upon receipt of an external force, capture electrical signals from the sensor's eight tip of the tactile wrists, and combining mapping and calibration with a multilayer perceptron (MLP), this results in an effective decoupling of the magnitude, position and direction of the 3D forces. To exemplify the concept of 3D force, we enveloped the bionic octopus-like sensor around a fingertip during writing. The sensor effectively detected the real-time force variations involved in the writing process. By leveraging the microcontroller's data acquisition and processing capabilities, eventually the written word can be reconstructed [35–37]. This demonstrates its potential use in high-precision intelligent writing recognition (Fig. 1b).

2. Experimental section

2.1. Synthesis of LIG/Ecoflex

The CO_2 laser marking machine (JTTS-ER, Jintai Laser Technology Co., Ltd.) was employed to produce LIG on a polyimide (PI) film of 0.025 mm thickness. This process was executed at a scanning speed of 18 mm/s, with a frequency of 100 kHz, and a power setting of 3.2 W. The laser's path was planned and controlled using CAD software. The aspect ratios of LIG strips are set to 20:1, 10:1 and 4:1 respectively, and the corresponding sizes are 15 mm × 0.75 mm, 15 mm × 1.5 mm and 15 mm × 3.75 mm. After that, the Ecoflex (Ecoflex™ 00–50, Smooth-On, Inc.), prepared at a mixing ratio of 1 A:1B, was gently and uniformly injected onto the LIG surface and the air was extracted from the Ecoflex mixture, thus facilitating complete penetration of the viscous Ecoflex into the 3D LIG network. The samples were then transferred to a convection oven to undergo cross-linking at 80 °C for 1 h. After it was completely cured, the LIG/Ecoflex was peeled off from the PI sheet (Fig. S1).

2.2. Fabrication of the octopus-like flexible 3D force sensor

Referring to the structure of octopus, eight-striped LIG with different aspect ratios was crafted using laser writing, followed by an Ecoflex transfer, thereby assembling the tactile wrists of the bionic octopus-like sensor (Fig. S2). Next, an annular mold featuring holes (inner diameter: 12 mm, depth: 3 mm) was placed at the center of the octopus tactile wrist layer. Then the uncured CNT/Ecoflex elastic composite (W_{CNTs}: $W_{Ecoflex}$=5%:95%) was poured, and the mold was withdrawn after the sample was cured. Each end of the eight LIG/Ecoflex tactile wrists was coated with conductive silver paste and connected to a copper wire, whereas the upper surface of the CNT/Ecoflex conductive elastomer was also coated with liquid metal to connect a copper wire. Finally, the

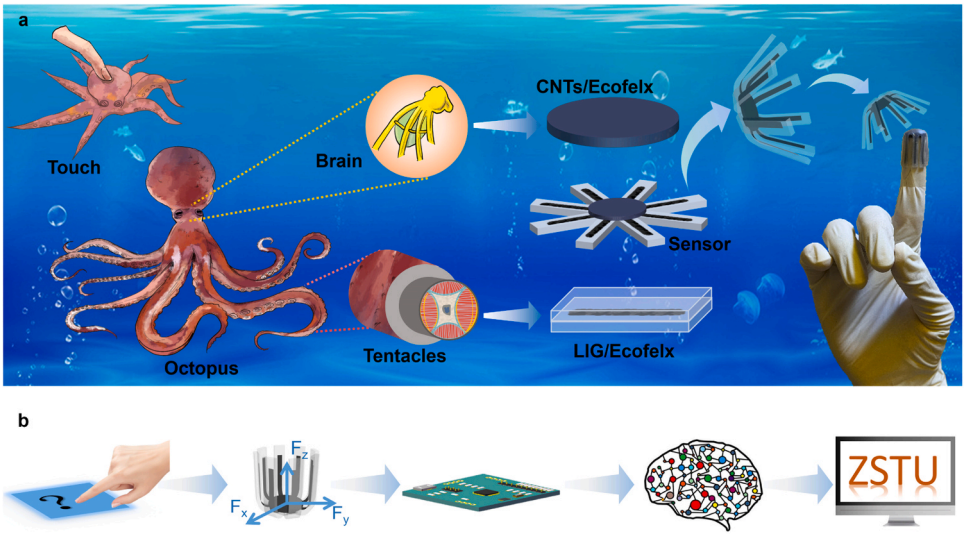

Fig. 1. The design concept and operating principle of bioinspired tactile sensors. (a) The sensor consists of a component that mimics the tactile ability of an octopus' body (centralized by the brain) and a component that mimics the tactile ability and shape of an octopus' tactile wrist, and then deforms to fit the shape of the fingertip for further tactile sensing. (b) Working principle of flexible 3D force sensor with biomimetic octopus structure for tactile sensing and recognition of fingertip writing.

sensor encapsulation was completed by using uncured Ecoflex to be poured onto the sensor surface and thermally cured. A cutting step subsequently leaded to the final bionic octopus-like flexible 3D force sensor (Fig. S1).

2.3. Measurement and characterization

The microstructures of LIG/Ecoflex and CNT/Ecoflex were analyzed using a scanning electron microscope (SEM, CARL ZEISS SMT PTE Ltd.) with an extra high voltage of 3 kV. The component and structure property of LIG/Ecoflex were analyzed by Raman spectrometer (LabRAM HR Evolution, HORIBA France SAS), FTIR spectrometer (Nicolet™iS50, Thermo Scientific™) and X-ray diffractometer (XRD, D8 DISCOVER, BRUKER). XRD used Cu Kα radiation ($\lambda = 0.15418$ nm) to perform 2θ scans from 10° to 80° in 0.2° steps. The force-electric test system including a mechanical testing machine (HY-0230, Yiheng precision instruments) was assembled for 3D force testing with varying degrees of incline. The resistance of the bionic octopus-like sensor under different testing conditions was captured using a Synchronous AD capture card (USB_HRF4028, Heng rui feng Measurement and Control Technology Co.).

2.4. Simulation

The strain distribution of the bionic octopus-like sensor was calculated using the finite element method (FEM). For the eight tactile wrists and head of the bionic octopus-like sensor, uniaxial test data from LIG/Ecoflex and CNTs/Ecoflex, respectively, were imported into the MatEditor of ANSYS and the experimental data were fitted using Mooney-Rivlin 2 parameter master model and Mooney-Rivlin 3 parameter master model. Importing model of the bionic octopus-like sensor into Simulation module of SOLIDWORKS, eight distal lower edges of the sensor tactile wrist were fixed and different loads were applied to the top of sensor. Accordingly, stress-strain relationships were obtained and finite element cloud maps were generated.

2.5. Neural networks

Two multilayer perceptron models were developed using Python in the PyTorch framework, both models have four fully connected layers and use rectified linear unit (ReLU) activation functions after each fully connected layers. The regression model is an MLP with 8 input features and 3 output features, which solves the decoupling of 3D forces and the verification of the radial distance (r). A multiclassification model was developed for the multiclassification problem. The multiclassification model is an MLP with 8 input features and 8 output features. This model uses a Softmax function after the final output layer which allows the output to be interpreted as a probability distribution. The multiclassification model is used to validate the parameters polar angle (θ) and azimuthal angle (φ).

3. Results and discussion

3.1. Microstructure of sensor

LIG is a top choice for creating flexible sensing materials, owing to its excellent electrical conductivity, remarkable strain sensitivity, programmable patterning design, and low cost [38–41]. The optical image of LIG, prepared via laser writing on PI, is displayed in Fig. S3a. The SEM characterization reveals LIG's unique 3D loose porous structure (Fig. S3b and Fig. S3c). Upon transferring LIG onto a flexible Ecoflex substrate (Fig. 2a), the SEM image demonstrates that the transferred LIG retains its inherent porous structure (Fig. 2b) [42]. Furthermore, the SEM cross-section image of the LIG/Ecoflex shows the tight bond

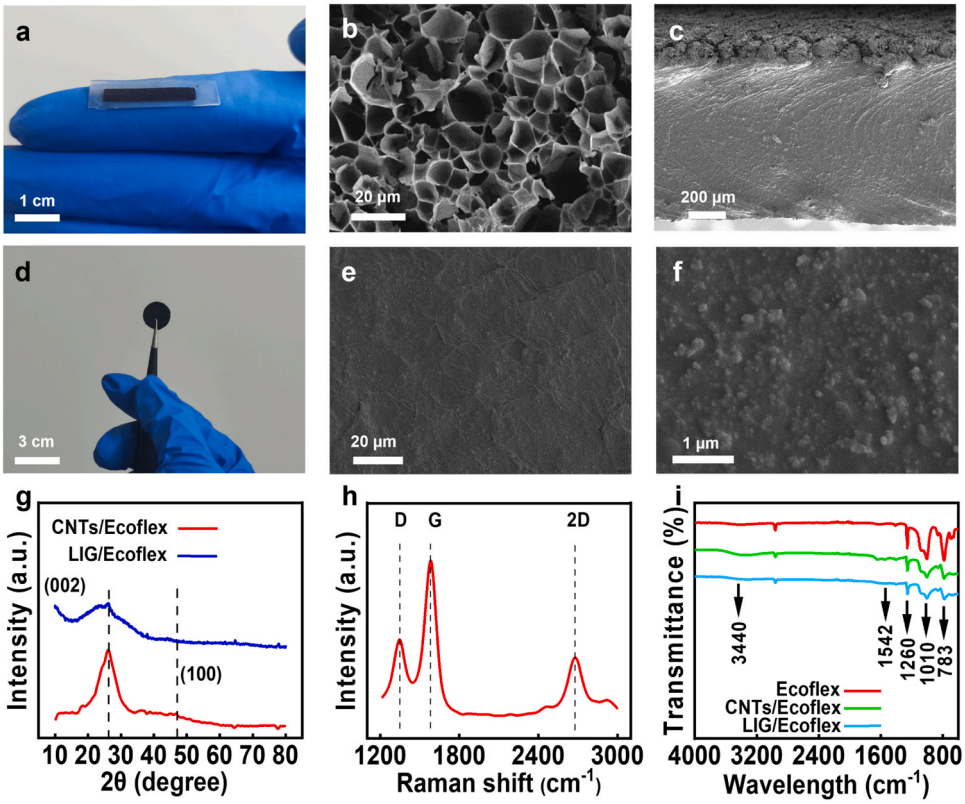

Fig. 2. Characterization of LIG/Ecoflex and CNTs/Ecoflex. (a) Digital photographs of the LIG/Ecoflex. (b and c) SEM images of LIG/Ecoflex. (d) Digital photographs of the CNTs/Ecoflex. (e and f) SEM images at different magnifications of CNTs/Ecoflex. (g) XRD diagram of the CNTs/Ecoflex and LIG/Ecoflex. (h) Raman diagram of the LIG. (i) FTIR diagrams of the pristine Ecoflex, CNTs/Ecoflex and LIG/Ecoflex.

between the Ecoflex and conductive LIG (Fig. 2c), contributing to LIG's flexibility and stretchability. The corresponding microcrack structures on the LIG surface is visible to the naked eye with the LIG/Ecoflex sample stretched to 100% (Fig. S4). When used as a flexible tactile wrist for the bionic octopus-like flexible 3D force sensor, LIG/Ecoflex can stretch up to 600% (Fig. S5). The LIG/Ecoflex tactile wrist effectively combines the benefits of Ecoflex and LIG, where the addition of Ecoflex improves the stretchability of LIG while maintaining the excellent conductivity of LIG (LIG/Ecoflex square resistance of 110.53 Ω cm).

CNT, which has excellent mechanical and electrical properties, is compounded with Ecoflex and made into a cylindrical elastomer that resembles the body of an octopus [43]. An optical photograph of the CNTs/Ecoflex material, with a light mass of 1.03 g cm^{-3}, is shown in Fig. 2d. SEM images of CNTs/Ecoflex (Fig. 2e and f) illustrate that the elastomers possess a wrinkled surface indicative of flexibility. The CNTs/Ecoflex mixture was poured into the center of the LIG/Ecoflex flexible tactile wrist layer within the constraints of the mold (Fig. S1), ensuring that the resulting bionic octopus flexible 3D force sensor maintains a robust electrical connection. The optical diagram of the fully prepared bionic octopus-like flexible 3D force sensor is presented in Fig. S6a, while the SEM characterization in Fig. S6b and Fig. S6c effectively demonstrates the connectivity between the body and tactile wrist sections of the sensor. The XRD spectra of LIG/Ecoflex show a prominent peak $2\theta = 25.9^{\circ}$ which corresponds to the (002) plane of LIG [38]. According to the Bragg's formula $n\lambda = 2l\sin\theta$ ($\lambda = 1.54$ Å is the X-ray wavelength, $\theta = 12.95^{\circ}$ is the incident contact angle, and $n = 1$ is the first-order diffraction), it can be concluded that the layer spacing of the LIG is $l = 3.436$ Å, which suggests that the LIG transfered to the surface of Ecoflex retained graphite structure. The Raman result of LIG (Fig. 2h) also shows three prominent characteristic peaks (D, G, and 2D) of graphene , and the D/G intensity ratio indicates a high degree of graphene formation within the LIG film [44]. The XRD pattern of LIG/Ecofelx (Fig. 2g) shows an intense peak centred at $2\theta = 25.9^{\circ}$, giving an interlayer spacing of ~3.4 Å between (002) planes in the LIG, and it also indicates the high degree of graphitization. The peak of LIG/Ecofelx at $\theta = 44^{\circ}$ is a (100) reflection associated with the in-plane structure. Influenced by slightly visible polymer background, the XRD pattern of CNTs/Ecoflex shows that the characteristic peaks of CNTs around 25.9° and 44° can still be distinguished after mixing of CNTs and Ecoflex, it is demonstrated that CNTs retain the crystalline state and are uniformly distributed in the Ecoflex matrix. In Fig. 2i, the FTIR spectroscopy of Ecoflex indicating four characteristic peaks can be characterized: the absorption peaks at 1010 cm^{-1}, 1260 cm^{-1}, 783 cm^{-1} and 3440 cm^{-1} indicate the main chains of Si-O-Si, Si-CH_3, Si-$(CH_3)_2$, and -OH, respectively [45]. When the CNTs are mixed into Ecoflex, the absorption peak of -OH increases significantly and a peak near 1542 cm^{-1} (vibrational mode of the CNTs tube wall, which indicates the presence of the graphitic structure of the CNTs) is introduced, which characterizes the fabrication of a homogeneous mixture of CNTs/Ecoflex material. While LIG is bound to the surface of Ecoflex, there is no chemical modification of the substrate, so no new functional groups are introduced, which allowes LIG/Ecoflex to maintain the excellent mechanical properties of Ecoflex.

3.2. Sensing performance

As structure determines performance, we first explored the effect of different aspect ratios of the sensor's eight tactile wrists on the sensor's electromechanical signals, specifically using LIG/Ecofelx tactile wrists with aspect ratios of 4:1, 10:1, and 20:1, respectively. As shown in Fig. S7, the sensor exhibits a large strain range with a resistance change of 60% when the aspect ratio is 4:1. However, the sensitivity is relatively low. Conversely, when the aspect ratio increased to 20:1, the sensor exhibited high sensitivity, but the effective strain range was limited to less than 5%. The optimal balance between sensitivity and effective strain range was achieved at an aspect ratio of 10:1. Hence, this aspect ratio was chosen for further experiments.

Strain range, sensitivity, and stability are three main indices to evaluate the strain-sensing performance of the sensor. Fig. 3d illustrates the electrical signal response of the LIG/Ecoflex flexible tactile wrists under both tension and bending. When stretched, LIG/Ecoflex produces a large number of microcracks with islands of conductive areas and greatly reduced conductive paths, resulting in a sharp increase in resistance (Fig. 3a). When bending, LIG/Ecoflex produces microcracks in the surface layer, but the deep conductive paths remain open, resulting in a much smaller change in resistance than when stretching (Fig. 3b) [46]. Notably, the Gauge Factor (GF) at 8%− 10% tensile strain measures at 573, emphasizing the high sensitivity of the LIG/Ecoflex when employed as a flexible tactile wrist. At a 10% tensile strain, the sensor exhibits a remarkable relative resistance change exceeding 2500%. In contrast, the impact on the electrical signal due to compressive deformation is virtually negligible, providing evidence for the effective decoupling of 3D forces. To assess the durability of the LIG/Ecoflex, the sensor's fatigue resistance is examined through 10,000 loading and unloading cycles, as depicted in Fig. 3e. The insets within the figure offer magnified views of the electrical signals around 2000, 5000, and 9000 cycles, demonstrating the sustained longevity and stability of the LIG/Ecoflex tactile wrist contact's electrical signals throughout numerous load and unload cycles. Shifting focus to Fig. 3f, the stress-strain curve of the LIG/Ecoflex is presented. Given the low modulus of elasticity of Ecoflex, the LIG/Ecoflex sensor exhibits susceptibility to deformation, leading to a discernible change in the electrical signal. This characteristic validates the source of the sensor's sensitivity. The response and recovery times (28 ms and 32 ms, respectively) are depicted in Fig. 3g, ensuring synchronized monitoring of external stimuli. Additionally, the reliable performance of LIG/Ecoflex at low frequencies is evident from the results in Fig. 3h. From the change in relative resistance of the CNTs/Ecoflex elastomers under compression (Fig. 3i), the resistance of the elastomers decreases as the compression intensifies, a phenomenon attributed to the increased density of CNTs in the elastomers during compression (Fig. 3c), and hence the increase in conductive pathways and decrease in resistance [47,48]. Similarly, the CNTs/Ecoflex elastomers showcase excellent stability and fatigue resistance properties during 10,000 compression load-unload cycles (Fig. 3j). The stress-strain curve of CNTs/Ecoflex (Fig. 3k) reveals that the elastomer is more susceptible to deformation in response to external stimuli and possesses a certain capacity to transmit loads [49]. This response successfully mimics the octopus body. Fig. 3l reports a response and recovery time (55 ms and 78 ms, respectively) that is comparable to that of LIG/Ecoflex, thus ensuring the coordination of signals between the two materials. The elastomer's compressive strain response is tested for 10 replicates at frequencies of 0.4, 0.33, 0.2, and 0.1 Hz. The response curves (Fig. 3m) demonstrate the sensor's commendable repeatability, with negligible interference from the loading frequency.

The assembled bionic octopus-like flexible sensor was tested for performance, as shown in Fig. S8. The sensor showed high sensitivity to load (GF= -0.116 N^{-1}) and fast response (29 ms) and recovery time (72 ms). The cyclic characteristics of the bionic octopus 3D force sensor in underwater operation were further explored (Fig. S9). The experimental results showed that due to the packaging process of Ecoflex, the sensor is guaranteed to maintain a high degree of signal stability and durability after more than 3000 cycles underwater. The basic performance of other flexible 3D force sensors was compared (Table S1), which verified the superiority of the bionic octopus 3D force sensor [27,50–54]. In addition, the effect of temperature change (from 20 °C to 60 °C) on the electrical performance of the sensor was also tested (Fig. S10). The observed resistance change (~0.04 at 60 °C) indicates the behavior of the sensor under temperature changing conditions. Importantly, we emphasize that in practical applications, where the ambient temperature generally does not exceed 40 °C, the corresponding resistance change of the sensor remains below 0.02. This change is

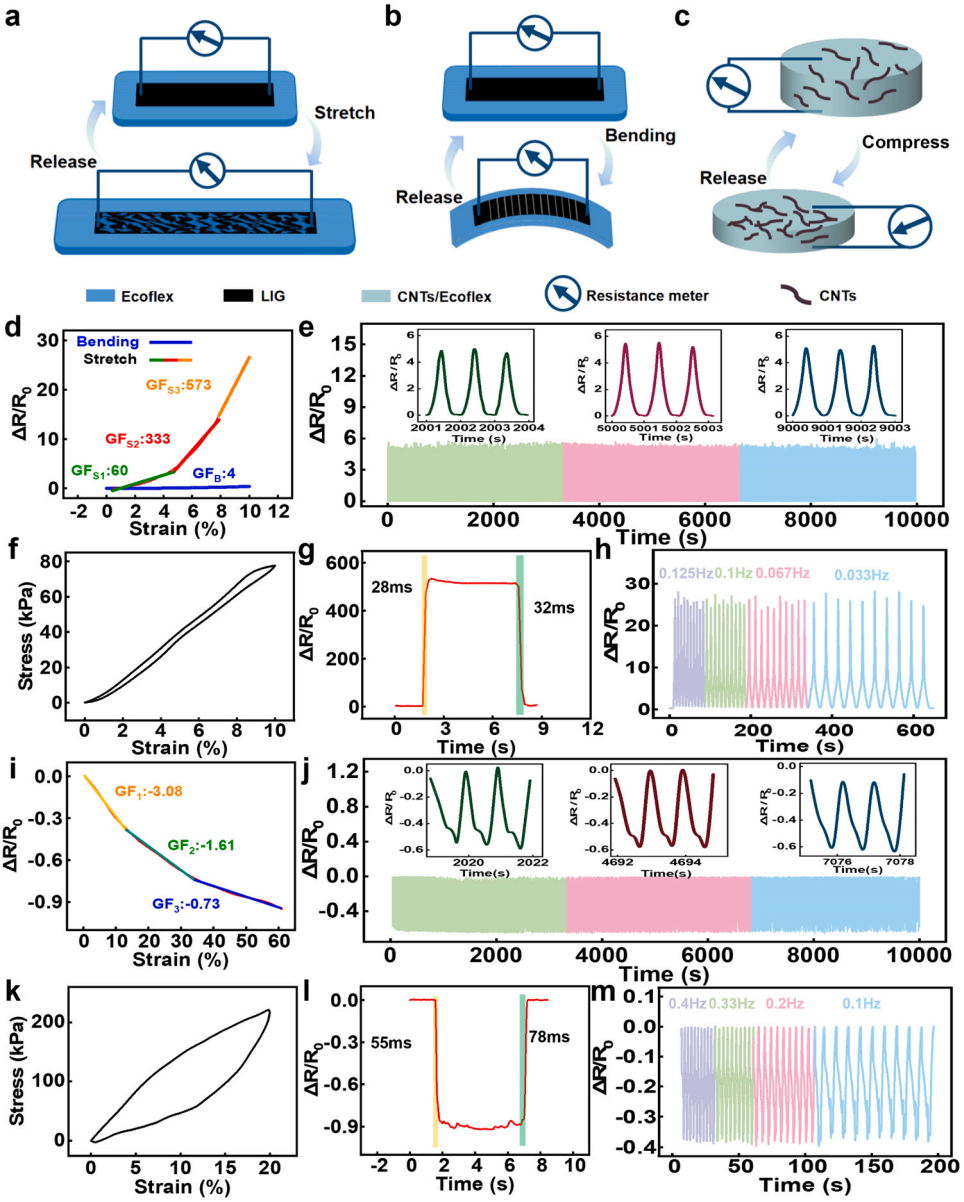

Fig. 3. Mechanical analysis and electromechanical testing of LIG/Ecoflex and CNT/Ecoflex sensor assemblies. (a) Schematic mechanism of LIG/Ecoflex uniaxial stretching. (b) Schematic diagram of the mechanism of LIG/Ecoflex compression bending. (c) Schematic diagram of the mechanism of CNTs/Ecoflex compression. (d) Relative resistance changes of LIG/Ecoflex sensors under uniaxial tensions in the linear stretching and linear bending. (e) Relative resistance variation with a cyclic strain of 5% for 10000 cycles of LIG/Ecoflex sensors. (f) Stress-strain curve of LIG/Ecoflex sensors under linear tensile uniaxial tension. (g) Response time and recovery time of LIG/Ecoflex sensors under linear tension uniaxial tension. (h) Relative resistance variation of LIG/Ecoflex sensors at different frequencies at 10% cyclic strain. (i) Relative resistance changes of CNTs/Ecoflex sensors under linear pressure uniaxial compression. (j) Relative resistance variation of CNTs/Ecoflex sensors with a cyclic compress of 25% for 10000 cycles. (k) Stress-strain curve of CNTs/Ecoflex sensors under linear pressure uniaxial compression. (l) Response time and recovery time of CNTs/Ecoflex sensors under linear pressure uniaxial compression. (m) Relative resistance variation of CNTs/Ecoflex sensors at different frequencies at 10% of cyclic compress.

negligible compared to the strain-induced change in the sensing signal. In particular, the sensor has a unique structural design that can adapt to complex environments and measure various complex curved surfaces, opening up a new direction for multi-dimensional force sensors.

3.3. Recognition of three-dimensional force

The bionic octopus-like flexible sensor owes its 3D force sensing ability to its unique bionic structure. When a force is applied to the sensor's body, it can precisely identify the magnitude, direction, and location of the applied force by detecting the changes in the electrical signals of its eight tactile wrists. To analyze the 3D force sensing mechanism, we designed three different external force loading methods. These methods included applying positive force to the body (Fig. 4a), applying positive force to the tactile wrists (Fig. 4d), and applying 3D force to the body (Fig. 4g). A mechanical testing machine was employed to quantitatively load the pressure, while a 3D printed inclined table was utilized for 3D force testing (Fig. S11). A Synchronous AD capture card was used to collect data. The positive force was measured by directly loading the corresponding force, and the 3D force was calculated by applying transformations to the test results from the inclined table. When a positive force of 1 N is applied to the top of the bionic octopus-like flexible sensor (Fig. 4a), the corresponding static finite element analysis cloud shows that the stress is concentrated in the sensor's body.

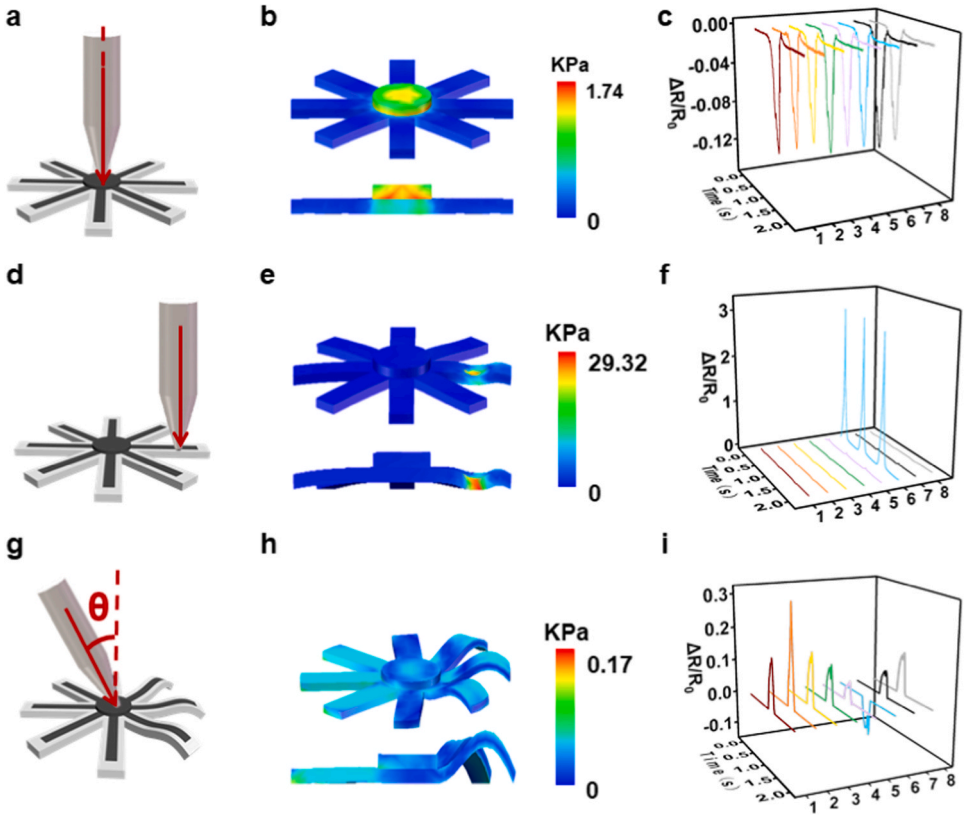

Fig. 4. Characteristics of the sensor response to positive force and 3D force. (a) Schematic diagram of positive force loading on the body of the bionic octopus-like sensor. (b) Mechanical finite element simulation of positive force loading on the body of a bionic octopus-like sensor. (c) Waterfall plot of the relative resistance change of the eight tactile wrists when positive force is applied to the body of the bionic octopus-like sensor. (d) Schematic diagram of positive force loading on the leg of the bionic octopus-like sensor. (e) Mechanical finite element simulation of positive force loading on the leg of a bionic octopus-like sensor. (f) Waterfall plot of the relative resistance change of the eight tactile wrists when positive force is applied to one tactile wrists of the bionic octopus-like sensor. (g) Schematic diagram of 3D forces loading on the body of the bionic octopus-like sensor. (h) Mechanical finite element simulation of 3D forces loading on the body of a bionic octopus-like sensor. (i) Waterfall plot of the relative resistance change of the eight tactile wrists when a 3D force is applied to the body of the bionic octopus-like sensor.

The positive force induces compression of the CNTs/Ecoflex elastomers and causes the tactile wrist's cracks to expand upon receiving pressure. This expansion results in an increase in electrical resistance, yet its contribution to the overall change in sensor resistance is negligible (Fig. 4b). The eight sets of sensor data obtained demonstrate a consistent magnitude of change, showing a 12% reduction in relative resistance (Fig. 4c). Conversely, in the control experimental group (Fig. S12a), which used a sensor devoid of CNTs/Ecoflex elastomers, the application of positive force yields a uniform 2% change in the electrical signals across the sensor's eight tactile wrists. This indicated that the positive force provides homogeneous electrical stimulation to the eight tactile wrists (Fig. S12b and c). Fig. S13a shows the electrical signals from one of the tactile wrists when different positive forces were applied to the sensor's body. The changes in the sensor's electrical signals progressively increase with the intensification of the positive force. To analyze the sensor's perception of 3D force, we marked the sensor's eight tactile wrists as shown in Fig. S14. Fig. 4d presents a schematic of a 1 N positive force applied to the bionic octopus tactile wrist #6. The cloud diagram of the static finite element analysis of the sensor (Fig. 4e) shows that the stresses are concentrated on the loaded tactile wrists, leading to a localized strain in the pressure [55]. The crack expansion of this tactile wrist results in a sharp increase in resistance, while no strain occurs in the CNTs/Ecoflex elastomer. Fig. 4f shows the change in sensor resistance during this load application, the resistance of the loaded tactile wrist #6 contact changes, resulting in a 300% increase in resistance at 1 N, while the other tactile wrists essentially exhibit no signal change.

The 3D force sensing capability of the bionic octopus-like sensor benefits from its unique bionic structure. As shown in Fig. S2, the different aspect ratios of the 3D force sensor tactile wrist obviously affect the sensor's electromechanical signals When 3D forces are applied to different sensors, increasing the aspect ratio increases the sensitivity of the sensor but at the expense of signal sensitivity; decreasing the aspect ratio results in a decrease in the sensitivity of the sensor. Therefore, the aspect ratio was determined to be 10:1 in the experiment, which can achieve the best balance between sensitivity and anti-interference characteristics, ensuring the effectiveness and resolution of 3D force decoupling. The bionic octopus-like sensor was examined for its ability to effectively recognize the position of the tactile wrist where the applied force is located. When a 3D force of 1 N is applied to the body of the bionic octopus (with normal angle $\theta = 30^{\circ}$, directed towards the tactile wrist #6) as shown in Fig. 4g, the corresponding static finite element analysis under this load reveals the generation of compressive strain on the sensor's body (Fig. 4h). As a result, the CNTs/Ecoflex elastomer is compressed and the piezoresistive effect leads to a reduction in the resistance of the elastomer. However, the strain experienced by the tactile wrist part of the bionic octopus-like sensor is primarily oriented along the directions of tactile wrists #2 and #6. Tactile wrist #2 undergoes tension, and the resulting crack expansion effect increases the resistance. On the other hand, tactile wrist #6 experiences compression and bending, which minimizes crack expansion and results in a relatively small increase in resistance. The remaining tactile wrists are symmetrically distributed around this direction, and the degree of strain they experience results in varying levels of resistance increase based on the amount of stress components (Fig. S12d-f). Fig. 4i illustrates the sensor's electrical response during this loading, with the eight sets of data variations symmetrically distributed around tactile wrists #2

and #6. This results in a 30% increase in resistance at 1 N in the circuit connected to tactile wrist #2, and a 10% decrease in resistance at tactile wrist #6. The electrical signals associated with tactile wrist #2 were evaluated by applying forces of 1 N, 2 N, and 3 N to the body of the bionic octopus-like sensor in the same direction. This demonstrates that the sensor shows a steady increase in the electrical signal change with increasing applied pressure (Fig. S13b). This can be attributed to the high strain sensitivity of both CNTs/Ecoflex and LIG/Ecoflex. Moreover, we conducted control experiments under two different conditions: with the same angle 30° but varying force application magnitudes (Fig. S15a and b), and with a consistent force application magnitude but at different tilt angles 45° (Fig. S15c and d). The eight sets of electrical signals generated across the three sets of experiments present regular variations. Taking the electrical signals of the maximally strained tactile wrist #2 as an illustration, when the applied 3D force is halved, the change in electrical signals from tactile wrist #2 also decrease by half. Furthermore, when the angle of the applied force is increased (45°), a shift in electrical signal from 30% to 50% is observed in tactile wrist #2.

Through the above modeling and analysis, we can derive several conclusions. First, the azimuth angle "φ" can be deduced from the alteration in the relative resistance of the primary strain direction of the tactile wrist upon contact. Next, the intensity of the circumferential force can be determined from the relative resistance change within both the joint contact tactile wrist's main strain direction and its symmetry direction. Finally, this allows us to further calculate both the actual magnitude of the radial distance "r" and polar angle "θ".

To improve the accuracy of 3D force decoupling, we utilized MLP model to train and decouple the parameters "r", "θ" and "φ" of the 3D force [56,57]. However, to facilitate the operation of the multilayer perceptron model, we converted the 3D force parameters "r", "θ" and "φ" from the spherical coordinate system to F_x, F_y, F_z in the cartesian coordinate system (Fig. S14). The sensor's decoupling process using regression model is as follows: Firstly, the experimental calibration data was biased, and a random selection of 80% of the data was used as training samples, while the remaining 20% served as test samples. We then constructed a column vector, comprising the electrical signals from the 8 sensing units, as an input vector. This column vector, $F = [x\ y\ z]^T$, consists of the corresponding Cartesian coordinate system parameters acting on the sensor coordinate origin, serving as the sensor system's output vector (Fig. 5a). Given the nonlinear and coupled characteristics of the 8-channel electrical signal, the hidden layer design required first expanding the size of the 8-channel data, then reducing it to extract as many hidden features from the input signal as possible [58,59]. We maintained three hidden layers during experiments to strike a balance between computational complexity and result accuracy. The hidden layer's size was set at 96, 192, 384, with a ReLU activation function operating between layers. The root means square error (RMSE) was used to quantify the output loss of the training sample, and the loss function was optimized by the gradient descent method [60]. The findings revealed that when the neural network underwent training for 200 steps, the error margin was reduced to 10^{-3} (Fig. 5b).

As a verification, we conducted multiclassification model training on "θ" and "φ" respectively using the control variable method , conducted regression model training on "r". The confusion matrix's training results validated that the bionic octopus-like sensor's eight tactile wrists correspond to the eight direction parameters "φ" with high accuracy (Fig. 5c). The biomimetic octopus-like sensor parameter "θ" confusion matrix (Fig. 5d) demonstrated an experimental error below 2%. When "θ" was set to 30°, with regression model the training error curve for the bionic octopus-like sensor parameter "r" demonstrated that the error

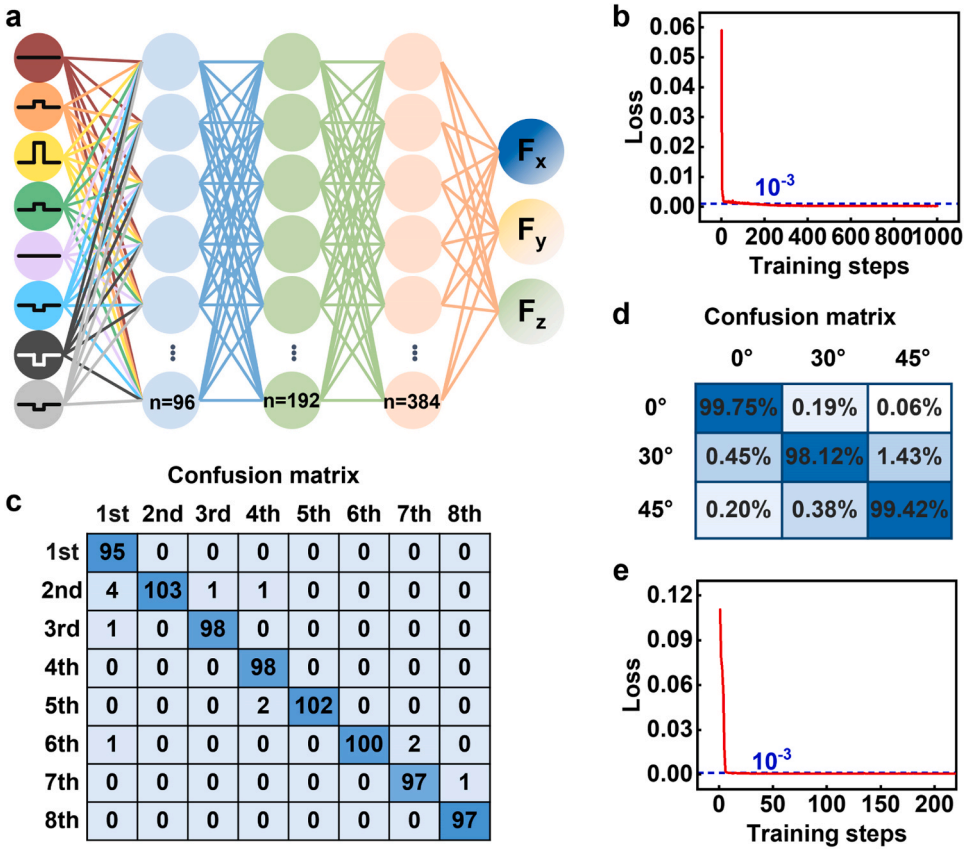

Fig. 5. ML for the bionic octopus-like sensor calibration. (a) Schematic diagram of multi-layer perceptron. (b) Training error curve of the bionic octopus-like sensor's 3D forces. (c) Confusion Matrix of the bionic octopus-like sensor parameter "φ". (d) Confusion matrix for the bionic octopus-like sensor parameter "θ". (e) Training error curve of the bionic octopus-like sensor's parameter "r" when "θ" is 30°.

could be reduced to the 10^{-3} level after merely 10 training cycles (Fig. 5e). Similarly, for "θ" set at 45°, we observed a comparable effect (Fig. S16). Consequently, multilayer perceptron model was leveraged to authenticate the accuracy of the 3D force parameters, thereby effectively facilitating the bionic octopus-like sensor's 3D force decoupling. This accomplishment significantly underscores the sensor's potential applicability in various domains such as robotics, wearable devices, and human-machine interfaces.

3.4. Application of bionic octopus-like sensor for handwriting recognition

In order to validate the concept of 3D force perception, we explored the potential application of the bionic octopus-like sensor in handwriting recognition (Fig. 6a). Referring to Fig. S14, the eight tactile wrists of the sensor were marked with corresponding colors. We wrapped the bionic octopus-like sensor around a fingertip and proceeded to write on a paper surface. The electrical signals from the eight tactile wrists were captured by a data acquisition card (at a frequency of 500 Hz), and the electrical response of writing was obtained by normalizing the sampled data. The basic strokes of writing include clockwise arcs, counterclockwise arcs, horizontal lines, vertical lines, apostrophe and downstroke. As depicted in the Fig. 6b-g, the group of eight electrical signals with the most substantial resistance change (the color corresponds to the tactile wrists) indicates the current writing direction. The variation of the negative electrical signal allows for determining the magnitude of the force value, with a larger change in the electrical signal signifying a larger force value. The writing process, from the initial application of force, to the phase of uniform force, and ultimately to the lifting of the finger (with no force application), exhibits a characteristic trapezoidal pattern in electrical signal changes [61].

Following the established pattern, we conducted an experiment by writing four letters, "Z S T U" (abbreviating Zhejiang Science and Technology University), and subsequently reconstructed their 3D diagrams (Fig. 6h-k). Taking the letter "U" as an example: the gray line corresponds to the bionic octopus's tactile wrist #8 sensing unit, signifying a downward writing motion from the fingertip. The end of this downward motion was overlaid by the electrical signal from the next tactile sensing unit, which was tactile wrist #7 sensing unit (black), indicating a rightward downward stroke from the fingertip. Then in order, the blue color corresponds to tactile wrist #6 (signifying a right stroke), the pink color corresponds to tactile wrist #5 (indicating an upper-right stroke), and the green color corresponds to tactile wrist #4 (signifying an upward stroke). The reconstructed 3D map reveals a coordination between the force-related variables and the strokes, and their projections can intuitively and accurately reflect the content of the writing. As a demonstration, we developed a human-computer interaction system integrating a bionic octopus 3D force sensor and a microcontroller. The microcontroller gathered changes in electrical signals during the process of handwriting (Fig. S17), which were then compared with the six basic strokes stored in the database. The results of the handwriting recognition were then displayed in real time via the MATLAB interface. Fig. 6l-o illustrates the application interface of the bionic octopus-like sensor in handwriting recognition of "ZSTU", and Video 1 demonstrates the dynamic, real-time display process within the MATLAB interface when the bionic octopus-like sensor was utilized to handwrite "ZSTU". Given that each individual possesses unique writing habits and that the force and speed of writing differ from person to person, the handwriting recognition system equipped with the bionic octopus-like 3D force sensor was capable of accurately recognizing and reconstructing the outcomes of the writing process. This system could therefore be leveraged as a significant tool for identity recognition.

Supplementary material related to this article can be found online at

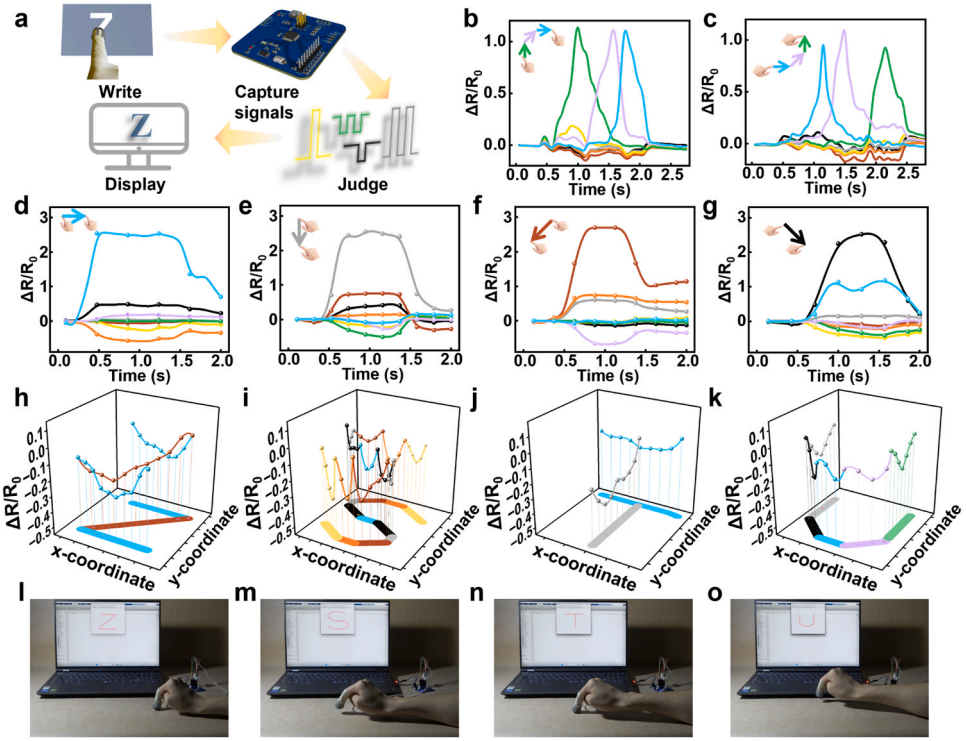

Fig. 6. Sensors for handwriting recognition. (a)Flow chart of bionic octopus-like sensor for fingertip writing. (b) Relative resistance change of the bionic octopus-like sensor when writing clockwise. (c) Relative resistance change of bionic octopus-like sensor when writing counterclockwise. (d) Relative resistance change of bionic octopus-like sensor when writing horizontally to the right. (e) Relative resistance change of bionic octopus-like sensor when writing vertically downward. (f) Relative resistance change of bionic octopus-like sensor when writing to the lower left. (g) Relative resistance change of bionic octopus-like sensor when writing to the lower right. (h, i, j, and k) Relative resistance change of the bionic octopus-like sensor when writing "Z", "S", "T" and "U". (l, m, n, and o) Displays an optical image of the writing result in real time.

doi:10.1016/j.nanoen.2024.109357.

4. Conclusion

We rationally designed and prepared a bionic octopus-like flexible 3D force sensor and explored its application to handwriting recognition. The material selection, the same Ecoflex substrate enables the material to have excellent flexibility and component compatibility. The normal and circumferential component forces are decoupled by an ingenious structural design, and the structure is beneficial for excellent fit on complex surfaces. The sensor's 3D force sensing capability has been demonstrated through testing, mechanical simulation and neural network validation. Thanks to these desirable properties, the sensor can successfully display handwriting content in real time and monitor changes in force during handwriting. This work demonstrates the application of sensors for 3D force monitoring, especially in the field of handwriting recognition.

CRediT authorship contribution statement

Ruan Diqing: Writing – original draft, Methodology, Investigation, Formal analysis, Data curation. **Liu Aiping:** Writing – review & editing, Supervision, Project administration, Funding acquisition. **Cheng Lin:** Writing – original draft, Supervision, Project administration. **Wu Huaping:** Methodology, Investigation, Conceptualization. **Luo Xuanzi:** Software, Investigation. **Chen Guanzheng:** Validation, Investigation.

Declaration of Competing Interest

The authors declare that they have no known competing financial interests or personal relationships that could have appeared to influence the work reported in this paper.

Data Availability

Data will be made available on request.

Acknowledgements

This work was supported by the National Natural Science Foundation of China (Nos. 12272351, 11972323 and 12372168), the Youth Top-notch Talent Project of Zhejiang Ten Thousand Plan of China (No. ZJWR0308010), the Zhejiang Provincial Natural Science Foundation of China (Nos. Z24A020008 and LR20A020002).

Appendix A. Supporting information

Supplementary data associated with this article can be found in the online version at doi:10.1016/j.nanoen.2024.109357.

References

[1] R. Zhang, M. Hummelgård, J. Örtegren, M. Olsen, H. Andersson, Y. Yang, H. Olin, Z.L. Wang, Utilising the triboelectricity of the human body for human-computer interactions, Nano Energy 100 (2022) 107503, https://doi.org/10.1016/j.nanoen.2022.107503.

[2] Y. Gao, L. Yu, J.C. Yeo, C.T. Lim, Flexible hybrid sensors for health monitoring: materials and mechanisms to render wearability, Adv. Mater. 32 (2020) e1902133, https://doi.org/10.1002/adma.201902133.

[3] L. Cheng, G.Q. Fang, L. Wei, W.Z. Gao, X.E. Wang, Z.H. Lv, W.J. Xu, C. Ding, H. P. Wu, A.P. Liu, Laser-induced graphene strain sensor for conformable lip-reading recognition and human–machine interaction, ACS Appl. Nano Mater. 6 (2023) 7290–7298, https://doi.org/10.1021/acsanm.3c00410.

[4] Y. Qiu, Y. Tian, S.S. Sun, J.H. Hu, Y.Y. Wang, Z. Zhang, A.P. Liu, H.Y. Cheng, W. Z. Gao, W.A. Zhang, H. Chai, H.P. Wu, Bioinspired, multifunctional dual-mode pressure sensors as electronic skin for decoding complex loading processes and human motions, Nano Energy 78 (2020) 105337, https://doi.org/10.1016/j.nanoen.2020.105337.

[5] L. Zhao, H. Tian, H. Liu, W. Zhang, F. Zhao, X. Song, J. Shao, Bio-inspired soft-rigid hybrid smart artificial muscle based on liquid crystal elastomer and helical metal wire, Small 19 (2023) 2206342, https://doi.org/10.1002/smll.202206342.

[6] X. Wang, J. Yang, K. Meng, Q. He, G. Zhang, Z. Zhou, X. Tan, Z. Feng, C. Sun, J. Yang, Z.L. Wang, Enabling the unconstrained epidermal pulse wave monitoring via finger-touching, Adv. Funct. Mater. 31 (2021) 2102378, https://doi.org/10.1002/adfm.202102378.

[7] X. Li, J. Cao, H. Li, P. Yu, Y. Fan, Y. Xiao, Y. Yin, X. Zhao, Z.L. Wang, G. Zhu, Differentiation of multiple mechanical stimuli by a flexible sensor using a dual-interdigital-electrode layout for bodily kinesthetic identification, ACS Appl. Mater. Interfaces 13 (2021) 26394–26403, https://doi.org/10.1021/acsami.1c05572.

[8] L. Cheng, D. Ruan, Y. He, J. Yang, W. Qian, L. Zhu, P. Zhu, H. Wu, A. Liu, A highly stretchable and sensitive strain sensor for lipreading extraction and speech recognition, J. Mater. Chem. C. 11 (2023) 8413–8422, https://doi.org/10.1039/D3TC01136D.

[9] C. Wan, G. Chen, Y. Fu, M. Wang, N. Matsuhisa, S. Pan, L. Pan, H. Yang, Q. Wan, L. Zhu, X. Chen, An artificial sensory neuron with tactile perceptual learning, Adv. Mater. 30 (2018) 1801291, https://doi.org/10.1002/adma.201801291.

[10] X. Chen, J. Shao, H. Tian, X. Li, C. Wang, Y. Luo, S. Li, Scalable imprinting of flexible multiplexed sensor arrays with distributed piezoelectricity-enhanced micropillars for dynamic tactile sensing, Adv. Mater. Technol. 5 (2020) 2000046, https://doi.org/10.1002/admt.202000046.

[11] M. Xu, J. Qi, F. Li, Y. Zhang, Transparent and flexible tactile sensors based on graphene films designed for smart panels, J. Mater. Sci. 53 (2018) 9589–9597, https://doi.org/10.1007/s10853-018-2216-5.

[12] S. Choi, K. Yoon, S. Lee, H.J. Lee, J. Lee, D.W. Kim, M.S. Kim, T. Lee, C. Pang, Conductive hierarchical hairy fibers for highly sensitive, stretchable, and water-resistant multimodal gesture-distinguishable sensor, VR applications, Adv. Funct. Mater. 29 (2019) 1905808, https://doi.org/10.1002/adfm.201905808.

[13] J. Li, C. Carlos, H. Zhou, J. Sui, Y. Wang, Z. Silva-Pedraza, F. Yang, Y. Dong, Z. Zhang, T.A. Hacker, B. Liu, Y. Mao, X. Wang, Stretchable piezoelectric biocrystal thin films, Nat. Commun. 14 (2023) 6562. ⟨https://www.nature.com/articles/s41467-023-42184-8⟩.

[14] Z. Zhang, G. Gu, W. Zhang, G. Gu, W. Shang, Y. Liu, G. Cheng, Z. Du, Double loops power management circuit of pulsed triboelectric nanogenerator with enhanced efficiency at low operating voltage and its application in self-powered flue gas monitoring system, Nano Energy 110 (2023) 108306, https://doi.org/10.1016/j.nanoen.2023.108360.

[15] L. Gong, N. Xuan, G. Gu, P. Lv, N. Huang, C. Song, M. Zheng, J. Wang, P. Cui, G. Gu, Y. Jia, G. Cheng, Z. Du, Power management and system optimization for high efficiency self-powered electrolytic hydrogen and formic acid production, Nano Energy 107 (2023) 108124, https://doi.org/10.1016/j.nanoen.2022.108124.

[16] L. Cheng, W. Qian, L. Wei, H. Zhang, T. Zhao, M. Li, A. Liu, H. Wu, A highly sensitive piezoresistive sensor with interlocked graphene microarrays for meticulous monitoring of human motions, J. Mater. Chem. C. 8 (2020) 11525–11531, https://doi.org/10.1039/d0tc02539a.

[17] Y. Qiu, C. Wang, X. Lu, H. Wu, X. Ma, J. Hu, H. Qi, Y. Tian, Z. Zhang, G. Bao, H. Chai, J. Song, A. Liu, A, A biomimetic drosera capensis with adaptive decision-predation behavior based on multifunctional sensing and fast actuating capability, Adv. Funct. Mater. 32 (2022) 2110296, https://doi.org/10.1002/adfm.202110296.

[18] G. Gu, G. Gu, W. Shang, Z. Zhang, W. Zhang, C. Wang, D. Fang, G. Cheng, Z. Du, The self-powered agricultural sensing system with 1.7 km wireless multichannel signal transmission using a pulsed triboelectric nanogenerator of corn husk composite film, Nano Energy 102 (2022) 107699, https://doi.org/10.1016/j.nanoen.2022.107699.

[19] S. Li, X. Chen, X. Li, H. Tian, C. Wang, B. Nie, J. He, J. Shao, Bioinspired robot skin with mechanically gated electron channels for sliding tactile perception, Sci. Adv. 8 (2022) eade0720. ⟨https://www.science.org/doi/10.1126/sciadv.ade0720⟩.

[20] Z. Zhang, G. Liu, Z. Li, W. Zhang, Q. Meng, Flexible tactile sensors with biomimetic microstructures: mechanisms, fabrication, and applications, Adv. Colloid Interface Sci. 320 (2023) 102988, https://doi.org/10.1016/j.cis.2023.102988.

[21] C. Mu, Y. Song, W. Huang, A. Ran, R. Sun, W. Xie, H. Zhang, Flexible normal-tangential force sensor with opposite resistance responding for highly sensitive artificial skin, Adv. Funct. Mater. 28 (2018) 1707503, https://doi.org/10.1002/adfm.201707503.

[22] C. Pang, G.-Y. Lee, T.-i Kim, S.M. Kim, H.N. Kim, S.-H. Ahn, K.-Y. Suh, A flexible and highly sensitive strain-gauge sensor using reversible interlocking of nanofibres, Nat. Mater. 11 (2012) 795–801, https://doi.org/10.1038/nmat3380.

[23] D. Kang, P.V. Pikhitsa, Y.W. Choi, C. Lee, S.S. Shin, L. Piao, B. Park, K.Y. Suh, T. I. Kim, M. Choi, Ultrasensitive mechanical crack-based sensor inspired by the spider sensory system, Nature 516 (2014) 222–226, https://doi.org/10.1038/nature14002.

[24] L. Liu, Y. Huang, F. Li, Y. Ma, W. Li, M. Su, X. Qian, W. Ren, K. Tang, Y. Song, Spider-web inspired multi-resolution graphene tactile sensor, ChemComm 54 (2018) 4810–4813, https://doi.org/10.1039/C8CC02339E.

[25] F. Sun, Y. Gu, Y. Cao, Q. Lu, Y. Bai, L. Li, M. Hao, C. Qu, S. Wang, L. Liu, T. Li, T. Zhang, Novel flexible pressure sensor combining with dynamic-time-warping algorithm for handwriting identification, Sens. Actuator A Phys. 293 (2019) 70–76, https://doi.org/10.1016/j.sna.2019.04.018.

[26] H. Luan, D. Zhang, Z. Xu, W. Zhao, C. Yang, X. Chen, MXene-based composite double-network multifunctional hydrogels as highly sensitive strain sensors, J. Mater. Chem. C. 10 (2022) 7604–7613, https://doi.org/10.1039/D2TC00679K.

[27] S. Chen, C. Bai, C. Zhang, D. Geng, R. Liu, Y. Xie, W. Zhou, Flexible piezoresistive three-dimensional force sensor based on interlocked structures, Sens. Actuator A Phys. 330 (2021) 112857, https://doi.org/10.1016/j.sna.2021.112857.
[28] G. Zhou, Z. Liao, R. Zhao, H. Yao, H. Dai, A force decoupling method for simultaneously measuring vertical and shear force, IEEE Sens. J. 22 (2022) 16820–16827, https://doi.org/10.1109/JSEN.2022.3192284.
[29] X.F. Zhao, X.H. Wen, P. Sun, C. Zeng, M.Y. Liu, F. Yang, H. Bi, D. Li, R.G. Ma, J. C. Wang, X.B. Yu, D.W. Zhang, H.L. Lu, Spider web-like flexible tactile sensor for pressure-strain simultaneous detection, ACS Appl. Mater. Interfaces 13 (2021) 10428–10436, https://doi.org/10.1021/acsami.0c21960.
[30] F. Ahmed, M. Waqas, B. Shaikh, U. Khan, A.M. Soomro, S. Kumar, H. Ashraf, F. H. Memon, K.H. Choi, Multi-material bio-inspired soft octopus robot for underwater synchronous swimming, J. Bionic Eng. 19 (2022) 1229–1241, https://doi.org/10.1007/s42235-022-00208-x.
[31] T. Gutnick, D. Rokhsar, M. Kuba, Cephalopod behaviour, Curr. Biol. 33 (2023) R1083–R1086, https://doi.org/10.1016/j.cub.2023.08.094.
[32] Z. Wang, Y. Yang, N. Li, T. Yao, J. An, Octopus-shaped self-powered motion sensor based on the triboelectric and piezoelectric effect, Mater. Technol. 37 (2021) 2001–2010, https://doi.org/10.1080/10667857.2021.1885227.
[33] Q. Xin, J. Zhang, Z. Han, H. Zhao, T. Hou, Y. Liu, S. Niu, Q. Han, Z. Mu, B. Li, Z. Wang, L. Ren, Advanced bio-inspired mechanical sensing technology: learning from nature but going beyond nature, Adv. Mater. Technol. 8 (2022) 2200756, https://doi.org/10.1002/admt.202200756.
[34] T. Gutnick, L. Zullo, B. Hochner, M. Kuba, Use of peripheral sensory information for central nervous control of arm movement by Octopus vulgaris, e3, Curr. Biol. 30 (2020) 4322–4327, https://doi.org/10.1016/j.cub.2020.08.037.
[35] Q. He, Z. Feng, X. Wang, Y. Wu, J. Yang, A smart pen based on triboelectric effects for handwriting pattern tracking and biometric identification, ACS Appl. Mater. Interfaces 14 (2022) 49295–49302, https://doi.org/10.1021/acsami.2c13714.
[36] Y. Liu, F. Zhuo, J. Zhou, L. Kuang, K. Tan, H. Lu, J. Cai, Y. Guo, R. Cao, Y. Fu, H. Duan, Machine-learning assisted handwriting recognition using graphene oxide-based hydrogel, ACS Appl. Mater. Interfaces 14 (2022) 54276–54286, https://doi.org/10.1021/acsami.2c17943.
[37] B. Nie, J. Geng, T. Yao, Y. Miao, Y. Zhang, X. Chen, J. Liu, Sensing arbitrary contact forces with a flexible porous dielectric elastomer, Mater. Horiz. 8 (2021) 962–971, https://doi.org/10.1039/D0MH01359E.
[38] M. Liu, J. Wu, H. Cheng, Effects of laser processing parameters on properties of laser-induced graphene by irradiating CO_2 laser on polyimide, Sci. China Technol. Sci. 65 (2021) 41–52, https://doi.org/10.1007/s11431-021-1918-8.
[39] A.F. Carvalho, A.J.S. Fernandes, C. Leitão, J. Deuermeier, A.C. Marques, R. Martins, E. Fortunato, F.M. Costa, Laser-induced graphene strain sensors produced by ultraviolet irradiation of polyimide, Adv. Funct. Mater. 28 (2018) 1805271, https://doi.org/10.1002/adfm.201805271.
[40] J. Lin, Z. Peng, Y. Liu, F. Ruiz-Zepeda, R. Ye, E.L. Samuel, M.J. Yacaman, B. I. Yakobson, J.M. Tour, Laser-induced porous graphene films from commercial polymers, Nat. Commun. 5 (2014) (2014) 5714, https://doi.org/10.1038/ncomms6714.
[41] L. Cheng, D. Ruan, Y. He, J. Yang, W. Qian, L. Zhu, P. Zhu, H. Wu, A. Liu, Highly stretchable and sensitive strain sensor for lip-reading extraction and speech recognition, J. Mater. Chem. C. 11 (2023) 8413–8422, https://doi.org/10.1039/d3tc01136d.
[42] R. Rahimi, M. Ochoa, W. Yu, B. Ziaie, Highly stretchable and sensitive unidirectional strain sensor via laser carbonization, ACS Appl. Mater. Inter. 7 (2015) 4463–4470, https://doi.org/10.1021/am509087u.
[43] P. Fryn, S. Lalik, N. Gorska, A. Iwan, M. Marzec, Comparison of the dielectric properties of Ecoflex((r)) with l,d-poly(lactic acid) or polycaprolactone in the presence of SWCN or 5CB, Materials 14 (2021) 1719, https://doi.org/10.3390/ma14071719.
[44] A.C. Ferrari, J.C. Meyer, V. Scardaci, C. Casiraghi, M. Lazzeri, F. Mauri, S. Piscanec, D. Jiang, K.S. Novoselov, S. Roth, A.K. Geim, Raman spectrum of graphene and graphene layers, Phys. Rev. Lett. 97 (2006) 187401, https://doi.org/10.1103/PhysRevLett.97.187401.
[45] Z. Zhang, T. Liang, Z. Jiang, X. Jiang, J. Hu, G. Pang, Application of infrared spectroscopy in research on aging of silicone rubber in harsh environment, Polymers 14 (2022) 4728, https://doi.org/10.3390/polym14214728.
[46] W. Wang, L. Lu, Z. Li, L. Lin, Z. Liang, X. Lu, Y. Xie, Fingerprint-inspired strain sensor with balanced sensitivity and strain range using laser-induced graphene, ACS Appl. Mater. Interfaces 14 (2022) 1315–1325, https://doi.org/10.1021/acsami.1c16646.
[47] G. Sudheer Kumar, T. Umasankar Patro, Tuning the piezoresistive strain-sensing behavior of poly (vinylidene fluoride)–CNT composites: the role of polymer–CNT interface and composite processing technique, J. Appl. Polym. Sci. 139 (3) (2022) 51516, https://doi.org/10.1002/app.51516.
[48] P. Francesco, Z. Michele, Q. Marino, Analytical model for the prediction of the piezoresistive behavior of CNT modified polymers, Compos. B. Eng. 109 (2017) 53–63, https://doi.org/10.1016/j.compositesb.2016.10.034.
[49] Y. Sliozberg, M. Kröger, T. Henry, S. Datta, B. Lawrence, A. Hall, A. Chattopadhyay, Computational design of shape memory polymer nanocomposites, Polymers 217 (2021) 123476, https://doi.org/10.1016/j.polymer.2021.123476.
[50] C. Zhang, R. Zhang, C. Ji, Z. Pei, Z. Fu, Y. Liu, S. Sang, R. Hao, Q. Zhang, Bioinspired crocodile skin-based flexible piezoelectric sensor for three-dimensional force detection, IEEE Sens. J. 23 (2023) 18, https://doi.org/10.1109/JSEN.2023.3301014.
[51] Y. Gong, X. Cheng, Z. Wu, Y. Liu, P. Yu, X. Hu, A flexible tactile sensor array for dynamic triaxial force measurement based on aligned piezoresistive nanofibers, IEEE Sens. J. 21 (2021) 19, https://doi.org/10.1109/JSEN.2021.3103781.
[52] J. Jin, S. Wang, D. Mei, C. Mao, Y. Wang, A novel flexible centralized force sensor based on tri-axis force refactoring method for arbitrary force components measurement, Adv. Intell. Syst 6 (2024) 1, https://doi.org/10.1002/aisy.202300213.
[53] D. Xu, B. Hu, G. Zheng, J. Wang, C. Li, Y. Zhao, Z. Yan, Z. Jiao, Y. Wu, M. Wang, H. Li, X. Guo, Sandwich-like flexible tactile sensor based on bioinspired honeycomb dielectric layer for three-axis force detection and robotic application, J. Mater. Sci. Mater. Electron. 34 (2023) 942, https://doi.org/10.1007/s10854-023-10336-7.
[54] P. Yu, F. Chen, J. Long, A three-dimensional force/temperature composite flexible sensor, Sens. Actuator A Phys. 365 (2024) 114891, https://doi.org/10.1016/j.sna.2023.114891.
[55] Y. Park, C. Franz, H. Ryu, H. Luan, K. Cotton, J. Kim, T. Chung, S. Zhao, A. Vazquez-Guardado, D. Yang, K. Li, R. Avila, J. Phillips, M. Quezada, H. Jang, S. Kwak, S. Won, K. Kwon, H. Jeong, A. Bandodkar, M. Han, H. Zhao, G. Osher, H. Wang, K. Lee, Y. Zhang, Y. Huang, J. Finan, J. Rogers, Three-dimensional, multifunctional neural interfaces for cortical spheroids and engineered assembloids, Sci. Adv. 7 (2021) 12, https://doi.org/10.1126/sciadv.abf9153.
[56] Y. Zhu, H. Luo, F. Zhao, R. Chen, Indoor/outdoor switching detection using multisensor DenseNet and LSTM, IEEE Internet Things J. 8 (2021) 1544–1556, https://doi.org/10.1109/JIOT.2020.3013853.
[57] V. Reddy, S. Melingi, C. Kumar, K. Kumar, R. Mojjada, Optimization driven spike deep belief neural network classifier: a deep-learning based multichannel spike sorting neural signal processor (NSP) module for high-channel-count brain machine interfaces (BMIs), Artif Intell Rev 56 (2023) 2207–2233, https://doi.org/10.1007/s10462-023-10575-4.
[58] Y. Lu, D. Kong, G. Yang, R. Wang, G. Pang, H. Luo, H. Yang, K. Xu, Machine learning-enabled tactile sensor design for dynamic touch decoding, Adv. Sci. 10 (2023) 2303949, https://doi.org/10.1002/advs.202303949.
[59] W. Liu, Y. Duo, X. Chen, B. Chen, T. Bu, L. Li, J. Duan, Z. Zuo, Y. Wang, B. Fang, F. Sun, K. Xu, X. Ding, C. Zhang, L. Wen, An intelligent robotic system capable of sensing and describing objects based on bimodal, self-powered flexible sensors, Adv. Funct. Mater. 33 (2023) 2306368, https://doi.org/10.1002/adfm.202306368.
[60] J. Hu, Y. Qiu, X. Wang, L. Jiang, X. Lu, M. Li, Z. Wang, K. Pang, Y. Tian, W. Zhang, Z. Xu, H. Zhang, H. Qi, A. Liu, Z. Zhang, H. Wu, Flexible six-dimensional force sensor inspired by the tenon-and-mortise structure of ancient Chinese architecture for orthodontics, Nano Energy 96 (2022) 107073, https://doi.org/10.1016/j.nanoen.2022.107073.
[61] H. Guo, J. Wan, H. Wang, H. Wu, C. Xu, L. Miao, M. Han, H. Zhang, Self-powered intelligent human-machine interaction for handwriting recognition, Research (2021) 689869, https://doi.org/10.34133/2021/4689869.

Diqing Ruan received his Bachelor of Engineering degree from Shenyang Aerospace University in 2020. He is currently studying for a master's degree at Zhejiang Sci-Tech University. His research interests are mainly in the development of flexible sensors based on multi-dimensional forces/strains to cope with complex external mechanical environments and flexible actuators to simulate external environments.

Guanzheng Chen received his B. S. degree from Zhejiang Sci-Tech University in 2022. He is currently studying in Zhejiang Sci-Tech University for his Master's degree. His research interests are developing novel materials for flexible sensors and their applications in wearable field.

Xuanzi Luo received his B. S. degree in Guangdong Polytechnic Normal University in 2022. He is now studying for Master's degree in Zhejiang Sci-Tech University. His research interests involve solving multidimensional force perception problems in flexible tactile sensors with dual mode.

Lin Cheng received her Ph.D. degree in Materials Science and Engineering from the Zhejiang Sci-Tech University in 2023 and a Bachelor's degree from Henan University in 2017. Since 2017 her has been working at the Department of Physics (Zhejiang Sci-Tech University), where her research mainly focuses on flexible sensors based on smart materials/structures and their applications in human-computer interaction.

Prof. Huaping Wu received his Ph. D. degree in Engineering Mechanics from the Harbin Institute of Technology in 2009 and a Bachelor's degree from the Harbin Institute of Technology in 2002. He worked as a visiting scholar at the Kyoto University in 2014 and a postdoctoral research fellow at the City University of Hong Kong in 2012. He is currently a Professor in the School of Mechanical Engineering at Zhejiang University of Technology. His research mainly focuses on the mechanics of smart materials/structures, bionic machinery and bionic manufacturing, and flexible electronics devices.

Prof. Aiping Liu received her Ph. D. degree in Material Science from the Harbin Institute of Technology in 2008. She worked as a postdoctoral research fellow at the Nanyang Technological University from 2009 to 2011 and a visiting scholar at the University of Texas at Austin from 2019 to 2020. She is currently a Professor in the Department of Physics at Zhejiang Sci-Tech University. Her research mainly focuses on functional inorganic/organic materials for wearable physical/chemical sensors and smart actuators.